Measurement of cross section of $e^+e^- \to \phi\pi^+\pi^-$ at center-of-mass energies $\sqrt{s}$=2.0000-3.0800 GeV

M. Ablikim[1], M. N. Achasov[10,c], P. Adlarson[67], S. Ahmed[15], M. Albrecht[4], R. Aliberti[28], A. Amoroso[66A,66C], M. R. An[32], Q. An[63,49], X. H. Bai[57], Y. Bai[48], O. Bakina[29], R. Baldini Ferroli[23A], I. Balossino[24A], Y. Ban[38,j], K. Begzsuren[26], N. Berger[28], M. Bertani[23A], D. Bettoni[24A], F. Bianchi[66A,66C], J. Bloms[60], A. Bortone[66A,66C], I. Boyko[29], R. A. Briere[5], H. Cai[68], X. Cai[1,49], A. Calcaterra[23A], G. F. Cao[1,54], N. Cao[1,54], S. A. Cetin[53A], J. F. Chang[1,49], W. L. Chang[1,54], G. Chelkov[29,b], D. Y. Chen[6], G. Chen[1], H. S. Chen[1,54], M. L. Chen[1,49], S. J. Chen[35], X. R. Chen[25], Y. B. Chen[1,49], Z. J Chen[20,k], W. S. Cheng[66C], G. Cibinetto[24A], F. Cossio[66C], X. F. Cui[36], H. L. Dai[1,49], X. C. Dai[1,54], A. Dbeyssi[15], R. E. de Boer[4], D. Dedovich[29], Z. Y. Deng[1], A. Denig[28], I. Denysenko[29], M. Destefanis[66A,66C], F. De Mori[66A,66C], Y. Ding[33], C. Dong[36], J. Dong[1,49], L. Y. Dong[1,54], M. Y. Dong[1,49,54], X. Dong[68], S. X. Du[71], Y. L. Fan[68], J. Fang[1,49], S. S. Fang[1,54], Y. Fang[1], R. Farinelli[24A], L. Fava[66B,66C], F. Feldbauer[4], G. Felici[23A], C. Q. Feng[63,49], J. H. Feng[50], M. Fritsch[4], C. D. Fu[1], Y. Gao[64], Y. Gao[38,j], Y. Gao[63,49], Y. G. Gao[6], I. Garzia[24A,24B], P. T. Ge[68], C. Geng[50], E. M. Gersabeck[58], A Gilman[61], K. Goetzen[11], L. Gong[33], W. X. Gong[1,49], W. Gradl[28], M. Greco[66A,66C], L. M. Gu[35], M. H. Gu[1,49], S. Gu[2], Y. T. Gu[13], C. Y Guan[1,54], A. Q. Guo[22], L. B. Guo[34], R. P. Guo[40], Y. P. Guo[9,h], A. Guskov[29,b], T. T. Han[41], W. Y. Han[32], X. Q. Hao[16], F. A. Harris[56], K. L. He[1,54], F. H. Heinsius[4], C. H. Heinz[28], T. Held[4], Y. K. Heng[1,49,54], C. Herold[51], M. Himmelreich[11,f], T. Holtmann[4], G. Y. Hou[1,54], Y. R. Hou[54], Z. L. Hou[1], H. M. Hu[1,54], J. F. Hu[47,l], T. Hu[1,49,54], Y. Hu[1], G. S. Huang[63,49], L. Q. Huang[64], X. T. Huang[41], Y. P. Huang[1], Z. Huang[38,j], T. Hussain[65], N. Hüsken[22,28], W. Ikegami Andersson[67], W. Imoehl[22], M. Irshad[63,49], S. Jaeger[4], S. Janchiv[26], Q. Ji[1], Q. P. Ji[16], X. B. Ji[1,54], X. L. Ji[1,49], Y. Y. Ji[41], H. B. Jiang[41], X. S. Jiang[1,49,54], J. B. Jiao[41], Z. Jiao[18], S. Jin[35], Y. Jin[57], M. Q. Jing[1,54], T. Johansson[67], N. Kalantar-Nayestanaki[55], X. S. Kang[33], R. Kappert[55], M. Kavatsyuk[55], B. C. Ke[43,1], I. K. Keshk[4], A. Khoukaz[60], P. Kiese[28], R. Kiuchi[1], R. Kliemt[11], L. Koch[30], O. B. Kolcu[53A,e], B. Kopf[4], M. Kuemmel[4], M. Kuessner[4], A. Kupsc[67], M. G. Kurth[1,54], W. Kühn[30], J. J. Lane[58], J. S. Lange[30], P. Larin[15], A. Lavania[21], L. Lavezzi[66A,66C], Z. H. Lei[63,49], H. Leithoff[28], M. Lellmann[28], T. Lenz[28], C. Li[39], C. H. Li[32], Cheng Li[63,49], D. M. Li[71], F. Li[1,49], G. Li[1], H. Li[63,49], H. Li[43], H. B. Li[1,54], H. J. Li[16], J. L. Li[41], J. Q. Li[4], J. S. Li[50], Ke Li[1], L. K. Li[1], Lei Li[3], P. R. Li[31,m,n], S. Y. Li[52], W. D. Li[1,54], W. G. Li[1], X. H. Li[63,49], X. L. Li[41], Xiaoyu Li[1,54], Z. Y. Li[50], H. Liang[1,54], H. Liang[63,49], H. Liang[27], Y. F. Liang[45], Y. T. Liang[25], G. R. Liao[12], L. Z. Liao[1,54], J. Libby[21], C. X. Lin[50], B. J. Liu[1], C. X. Liu[1], D. Liu[15,63], F. H. Liu[44], Fang Liu[1], Feng Liu[6], H. B. Liu[13], H. M. Liu[1,54], Huanhuan Liu[1], Huihui Liu[17], J. B. Liu[63,49], J. L. Liu[64], J. Y. Liu[1,54], K. Liu[1], K. Y. Liu[33], L. Liu[63,49], M. H. Liu[9,h], P. L. Liu[1], Q. Liu[68], Q. Liu[54], S. B. Liu[63,49], Shuai Liu[46], T. Liu[1,54], W. M. Liu[63,49], X. Liu[31,m,n], Y. Liu[31,m,n], Y. B. Liu[36], Z. A. Liu[1,49,54], Z. Q. Liu[41], X. C. Lou[1,49,54], F. X. Lu[50], H. J. Lu[18], J. D. Lu[1,54], J. G. Lu[1,49], X. L. Lu[1], Y. Lu[1], Y. P. Lu[1,49], C. L. Luo[34], M. X. Luo[70], P. W. Luo[50], T. Luo[9,h], X. L. Luo[1,49], X. R. Lyu[54], F. C. Ma[33], H. L. Ma[1], L. L. Ma[41], M. M. Ma[1,54], Q. M. Ma[1], R. Q. Ma[1,54], R. T. Ma[54], X. X. Ma[1,54], X. Y. Ma[1,49], F. E. Maas[15], M. Maggiora[66A,66C], S. Maldaner[4], S. Malde[61], A. Mangoni[23B], Y. J. Mao[38,j], Z. P. Mao[1], S. Marcello[66A,66C], Z. X. Meng[57], J. G. Messchendorp[55], G. Mezzadri[24A], T. J. Min[35], R. E. Mitchell[22], X. H. Mo[1,49,54], Y. J. Mo[6], N. Yu. Muchnoi[10,c], H. Muramatsu[59], S. Nakhoul[11,f], Y. Nefedov[29], F. Nerling[11,f], I. B. Nikolaev[10,c], Z. Ning[1,49], S. Nisar[8,i], S. L. Olsen[54], Q. Ouyang[1,49,54], S. Pacetti[23B,23C], X. Pan[9,h], Y. Pan[58], A. Pathak[1], P. Patteri[23A], M. Pelizaeus[4], H. P. Peng[63,49], K. Peters[11,f], J. Pettersson[67], J. L. Ping[34], R. G. Ping[1,54], S. Pogodin[29], R. Poling[59], V. Prasad[63,49], H. Qi[63,49], H. R. Qi[52], K. H. Qi[25], M. Qi[35], T. Y. Qi[9], S. Qian[1,49], W. B. Qian[54], Z. Qian[50], C. F. Qiao[54], L. Q. Qin[12], X. P. Qin[9], X. S. Qin[41], Z. H. Qin[1,49], J. F. Qiu[1], S. Q. Qu[36], K. H. Rashid[65], K. Ravindran[21], C. F. Redmer[28], A. Rivetti[66C], V. Rodin[55], M. Rolo[66C], G. Rong[1,54], Ch. Rosner[15], M. Rump[60], H. S. Sang[63], A. Sarantsev[29,d], Y. Schelhaas[28], C. Schnier[4], K. Schoenning[67], M. Scodeggio[24A,24B], D. C. Shan[46], W. Shan[19], X. Y. Shan[63,49], J. F. Shangguan[46], M. Shao[63,49], C. P. Shen[9], H. F. Shen[1,54], P. X. Shen[36], X. Y. Shen[1,54], H. C. Shi[63,49], R. S. Shi[1,54], X. Shi[1,49], X D Shi[63,49], J. J. Song[41], W. M. Song[27,1], Y. X. Song[38,j], S. Sosio[66A,66C], S. Spataro[66A,66C], K. X. Su[68], P. P. Su[46], F. F. Sui[41], G. X. Sun[1], H. K. Sun[1], J. F. Sun[16], L. Sun[68], S. S. Sun[1,54], T. Sun[1,54], W. Y. Sun[34], W. Y. Sun[27], X Sun[20,k], Y. J. Sun[63,49], Y. K. Sun[63,49], Y. Z. Sun[1], Z. T. Sun[1], Y. H. Tan[68], Y. X. Tan[63,49], C. J. Tang[45], G. Y. Tang[1], J. Tang[50], J. X. Teng[63,49], V. Thoren[67], W. H. Tian[43], Y. T. Tian[25], I. Uman[53B], B. Wang[1], C. W. Wang[35], D. Y. Wang[38,j], H. J. Wang[31,m,n], H. P. Wang[1,54], K. Wang[1,49], L. L. Wang[1], M. Wang[41], M. Z. Wang[38,j], Meng Wang[1,54], W. Wang[50], W. H. Wang[68], W. P. Wang[63,49], X. Wang[38,j], X. F. Wang[31,m,n], X. L. Wang[9,h], Y. Wang[50], Y. Wang[63,49], Y. D. Wang[37], Y. F. Wang[1,49,54], Y. Q. Wang[1], Y. Y. Wang[31,m,n], Z. Wang[1,49], Z. Y. Wang[1], Ziyi Wang[54],

Zongyuan Wang[1,54], D. H. Wei[12], F. Weidner[60], S. P. Wen[1], D. J. White[58], U. Wiedner[4], G. Wilkinson[61], M. Wolke[67], L. Wollenberg[4], J. F. Wu[1,54], L. H. Wu[1], L. J. Wu[1,54], X. Wu[9,h], Z. Wu[1,49], L. Xia[63,49], H. Xiao[9,h], S. Y. Xiao[1], Z. J. Xiao[34], X. H. Xie[38,j], Y. G. Xie[1,49], Y. H. Xie[6], T. Y. Xing[1,54], G. F. Xu[1], Q. J. Xu[14], W. Xu[1,54], X. P. Xu[46], Y. C. Xu[54], F. Yan[9,h], L. Yan[9,h], W. B. Yan[63,49], W. C. Yan[71], Xu Yan[46], H. J. Yang[42,g], H. X. Yang[1], L. Yang[43], S. L. Yang[54], Y. X. Yang[12], Yifan Yang[1,54], Zhi Yang[25], M. Ye[1,49], M. H. Ye[7], J. H. Yin[1], Z. Y. You[50], B. X. Yu[1,49,54], C. X. Yu[36], G. Yu[1,54], J. S. Yu[20,k], T. Yu[64], C. Z. Yuan[1,54], L. Yuan[2], X. Q. Yuan[38,j], Y. Yuan[1], Z. Y. Yuan[50], C. X. Yue[32], A. Yuncu[53A,a], A. A. Zafar[65], Zeng[6], Y. Zeng[20,k], A. Q. Zhang[1], B. X. Zhang[1], Guangyi Zhang[16], H. Zhang[63], H. H. Zhang[27], H. H. Zhang[50], H. Y. Zhang[1,49], J. J. Zhang[43], J. L. Zhang[69], J. Q. Zhang[34], J. W. Zhang[1,49,54], J. Y. Zhang[1], J. Z. Zhang[1,54], Jianyu Zhang[1,54], Jiawei Zhang[1,54], L. M. Zhang[52], L. Q. Zhang[50], Lei Zhang[35], S. Zhang[50], S. F. Zhang[35], Shulei Zhang[20,k], X. D. Zhang[37], X. Y. Zhang[41], Y. Zhang[61], Y. H. Zhang[1,49], Y. T. Zhang[63,49], Yan Zhang[63,49], Yao Zhang[1], Z. H. Zhang[6], Z. Y. Zhang[68], G. Zhao[1], J. Zhao[32], J. Y. Zhao[1,54], J. Z. Zhao[1,49], Lei Zhao[63,49], Ling Zhao[1], M. G. Zhao[36], Q. Zhao[1], S. J. Zhao[71], Y. B. Zhao[1,49], Y. X. Zhao[25], Z. G. Zhao[63,49], A. Zhemchugov[29,b], B. Zheng[64], J. P. Zheng[1,49], Y. Zheng[38,j], Y. H. Zheng[54], B. Zhong[34], C. Zhong[64], L. P. Zhou[1,54], Q. Zhou[1,54], X. Zhou[68], X. K. Zhou[54], X. R. Zhou[63,49], X. Y. Zhou[32], A. N. Zhu[1,54], J. Zhu[36], K. Zhu[1], K. J. Zhu[1,49,54], S. H. Zhu[62], T. J. Zhu[69], W. J. Zhu[9,h], W. J. Zhu[36], Y. C. Zhu[63,49], Z. A. Zhu[1,54], B. S. Zou[1], J. H. Zou[1]

(BESIII Collaboration)

[1] *Institute of High Energy Physics, Beijing 100049, People's Republic of China*
[2] *Beihang University, Beijing 100191, People's Republic of China*
[3] *Beijing Institute of Petrochemical Technology, Beijing 102617, People's Republic of China*
[4] *Bochum Ruhr-University, D-44780 Bochum, Germany*
[5] *Carnegie Mellon University, Pittsburgh, Pennsylvania 15213, USA*
[6] *Central China Normal University, Wuhan 430079, People's Republic of China*
[7] *China Center of Advanced Science and Technology, Beijing 100190, People's Republic of China*
[8] *COMSATS University Islamabad, Lahore Campus, Defence Road, Off Raiwind Road, 54000 Lahore, Pakistan*
[9] *Fudan University, Shanghai 200443, People's Republic of China*
[10] *G.I. Budker Institute of Nuclear Physics SB RAS (BINP), Novosibirsk 630090, Russia*
[11] *GSI Helmholtzcentre for Heavy Ion Research GmbH, D-64291 Darmstadt, Germany*
[12] *Guangxi Normal University, Guilin 541004, People's Republic of China*
[13] *Guangxi University, Nanning 530004, People's Republic of China*
[14] *Hangzhou Normal University, Hangzhou 310036, People's Republic of China*
[15] *Helmholtz Institute Mainz, Staudinger Weg 18, D-55099 Mainz, Germany*
[16] *Henan Normal University, Xinxiang 453007, People's Republic of China*
[17] *Henan University of Science and Technology, Luoyang 471003, People's Republic of China*
[18] *Huangshan College, Huangshan 245000, People's Republic of China*
[19] *Hunan Normal University, Changsha 410081, People's Republic of China*
[20] *Hunan University, Changsha 410082, People's Republic of China*
[21] *Indian Institute of Technology Madras, Chennai 600036, India*
[22] *Indiana University, Bloomington, Indiana 47405, USA*
[23] *INFN Laboratori Nazionali di Frascati , (A)INFN Laboratori Nazionali di Frascati, I-00044, Frascati, Italy; (B)INFN Sezione di Perugia, I-06100, Perugia, Italy; (C)University of Perugia, I-06100, Perugia, Italy*
[24] *INFN Sezione di Ferrara, (A)INFN Sezione di Ferrara, I-44122, Ferrara, Italy; (B)University of Ferrara, I-44122, Ferrara, Italy*
[25] *Institute of Modern Physics, Lanzhou 730000, People's Republic of China*
[26] *Institute of Physics and Technology, Peace Ave. 54B, Ulaanbaatar 13330, Mongolia*
[27] *Jilin University, Changchun 130012, People's Republic of China*
[28] *Johannes Gutenberg University of Mainz, Johann-Joachim-Becher-Weg 45, D-55099 Mainz, Germany*
[29] *Joint Institute for Nuclear Research, 141980 Dubna, Moscow region, Russia*
[30] *Justus-Liebig-Universitaet Giessen, II. Physikalisches Institut, Heinrich-Buff-Ring 16, D-35392 Giessen, Germany*
[31] *Lanzhou University, Lanzhou 730000, People's Republic of China*
[32] *Liaoning Normal University, Dalian 116029, People's Republic of China*
[33] *Liaoning University, Shenyang 110036, People's Republic of China*
[34] *Nanjing Normal University, Nanjing 210023, People's Republic of China*

[35] Nanjing University, Nanjing 210093, People's Republic of China
[36] Nankai University, Tianjin 300071, People's Republic of China
[37] North China Electric Power University, Beijing 102206, People's Republic of China
[38] Peking University, Beijing 100871, People's Republic of China
[39] Qufu Normal University, Qufu 273165, People's Republic of China
[40] Shandong Normal University, Jinan 250014, People's Republic of China
[41] Shandong University, Jinan 250100, People's Republic of China
[42] Shanghai Jiao Tong University, Shanghai 200240, People's Republic of China
[43] Shanxi Normal University, Linfen 041004, People's Republic of China
[44] Shanxi University, Taiyuan 030006, People's Republic of China
[45] Sichuan University, Chengdu 610064, People's Republic of China
[46] Soochow University, Suzhou 215006, People's Republic of China
[47] South China Normal University, Guangzhou 510006, People's Republic of China
[48] Southeast University, Nanjing 211100, People's Republic of China
[49] State Key Laboratory of Particle Detection and Electronics, Beijing 100049, Hefei 230026, People's Republic of China
[50] Sun Yat-Sen University, Guangzhou 510275, People's Republic of China
[51] Suranaree University of Technology, University Avenue 111, Nakhon Ratchasima 30000, Thailand
[52] Tsinghua University, Beijing 100084, People's Republic of China
[53] Turkish Accelerator Center Particle Factory Group, (A)Istanbul Bilgi University, 34060 Eyup, Istanbul, Turkey; (B)Near East University, Nicosia, North Cyprus, Mersin 10, Turkey
[54] University of Chinese Academy of Sciences, Beijing 100049, People's Republic of China
[55] University of Groningen, NL-9747 AA Groningen, The Netherlands
[56] University of Hawaii, Honolulu, Hawaii 96822, USA
[57] University of Jinan, Jinan 250022, People's Republic of China
[58] University of Manchester, Oxford Road, Manchester, M13 9PL, United Kingdom
[59] University of Minnesota, Minneapolis, Minnesota 55455, USA
[60] University of Muenster, Wilhelm-Klemm-Str. 9, 48149 Muenster, Germany
[61] University of Oxford, Keble Rd, Oxford, UK OX13RH
[62] University of Science and Technology Liaoning, Anshan 114051, People's Republic of China
[63] University of Science and Technology of China, Hefei 230026, People's Republic of China
[64] University of South China, Hengyang 421001, People's Republic of China
[65] University of the Punjab, Lahore-54590, Pakistan
[66] University of Turin and INFN, (A)University of Turin, I-10125, Turin, Italy; (B)University of Eastern Piedmont, I-15121, Alessandria, Italy; (C)INFN, I-10125, Turin, Italy
[67] Uppsala University, Box 516, SE-75120 Uppsala, Sweden
[68] Wuhan University, Wuhan 430072, People's Republic of China
[69] Xinyang Normal University, Xinyang 464000, People's Republic of China
[70] Zhejiang University, Hangzhou 310027, People's Republic of China
[71] Zhengzhou University, Zhengzhou 450001, People's Republic of China

[a] Also at Bogazici University, 34342 Istanbul, Turkey
[b] Also at the Moscow Institute of Physics and Technology, Moscow 141700, Russia
[c] Also at the Novosibirsk State University, Novosibirsk, 630090, Russia
[d] Also at the NRC "Kurchatov Institute", PNPI, 188300, Gatchina, Russia
[e] Also at Istanbul Arel University, 34295 Istanbul, Turkey
[f] Also at Goethe University Frankfurt, 60323 Frankfurt am Main, Germany
[g] Also at Key Laboratory for Particle Physics, Astrophysics and Cosmology, Ministry of Education; Shanghai Key Laboratory for Particle Physics and Cosmology; Institute of Nuclear and Particle Physics, Shanghai 200240, People's Republic of China
[h] Also at Key Laboratory of Nuclear Physics and Ion-beam Application (MOE) and Institute of Modern Physics, Fudan University, Shanghai 200443, People's Republic of China
[i] Also at Harvard University, Department of Physics, Cambridge, MA, 02138, USA
[j] Also at State Key Laboratory of Nuclear Physics and Technology,

Peking University, Beijing 100871, People's Republic of China
[k] *Also at School of Physics and Electronics, Hunan University, Changsha 410082, China*
[l] *Also at Guangdong Provincial Key Laboratory of Nuclear Science, Institute of Quantum Matter, South China Normal University, Guangzhou 510006, China*
[m] *Also at Frontiers Science Center for Rare Isotopes, Lanzhou University, Lanzhou 730000, People's Republic of China*
[n] *Also at Lanzhou Center for Theoretical Physics, Lanzhou University, Lanzhou 730000, People's Republic of China*

(Dated: December 28, 2021)

Using data corresponding to an integrated luminosity of 651 pb^{-1} accumulated at 22 center-of-mass energy points between 2.0000 and 3.0800 GeV by the BESIII experiment, the process $e^+e^- \to \phi\pi^+\pi^-$ is studied. The Born cross sections for $e^+e^- \to \phi\pi^+\pi^-$ are consistent with previous results, but with improved precision. A fit to the cross section is performed, which reveals contributions from two structures: the first one has a mass of M = $(2158^{+30}_{-33} \pm 4)$ MeV/c^2 and a width of $\Gamma = (218^{+81}_{-64} \pm 5)$ MeV, and the second one has a mass of M = $(2298^{+60}_{-44} \pm 6)$ MeV/c^2 and a width of $\Gamma = (219^{+117}_{-112} \pm 6)$ MeV, where the first uncertainties are statistical and the second systematic.

I. INTRODUCTION

The study of the hadron spectrum is important to understand the non-perturbative behavior of quantum chromodynamics (QCD). For the low-energy region, the vector mesons ρ, ω, ϕ and their low-lying excited states are copiously produced in e^+e^- collision experiments. The experimental results for these states have been tabulated by the Particle Data Group (PDG) [1], but the higher lying excitations are not fully identified yet, especially in the region around 2 GeV. Further measurements are needed to resolve the situation involving resonances such as the $\rho(2000)$, $\rho(2150)$ and $\phi(2170)$ states.

The $\phi(2170)$ resonance was first observed by the BABAR Collaboration via the initial-state-radiation (ISR) process $e^+e^- \to \gamma_{ISR}\phi f_0(980)$ [2], and later confirmed by the Belle, BESII, and BESIII experiments [3–7]. This observation stimulated speculation that the $\phi(2170)$ resonance might be a strangeonium counterpart of the charmonium resonance $\psi(4260)$ due to similarities in their production and decay pattern [8]. Considerable efforts have been made theoretically to understand the nature of the $\phi(2170)$ resonance and abundant interpretations have been proposed, including a traditional $s\bar{s}$ state [9–14], an $s\bar{s}g$ hybrid [8, 15], an $ss\bar{s}\bar{s}$ tetra-quark state [16–23], a $\Lambda\bar{\Lambda}$ bound state [24–28] and an ordinary $\phi K\bar{K}$ or $\phi f_0(980)$ resonance produced by interactions between the final state particles [29, 30]. The model predictions differ in both mass and width of the resonance. Further experimental studies are therefore crucial to clarify its nature.

Though many experiments have been carried out to study the $\phi(2170)$ resonance [2–7, 31], the results of the measurements vary substantially. For example, the mass and width of the $\phi(2170)$ resonance obtained from the process $e^+e^- \to \gamma_{ISR}\phi\pi^+\pi^-$ [4] shows smaller values than other experimental measurements. Recently, more studies related to the $\phi(2170)$ resonance have been carried out by the BESIII experiment. A partial-wave analysis of the $e^+e^- \to K^+K^-\pi^0\pi^0$ process [32] found that the partial widths of the $\phi(2170)$ resonance are sizable for the $K(1460)^+K^-$, $K_1(1400)^+K^-$, and $K_1(1270)^+K^-$ decay channels, but much smaller for $K^*(892)^+K^*(892)^-$ and $K^*(1410)^+K^-$. Several theoretical expectations are challenged by the results according to Ref. [9]. Attempts have also been made to study channels with simpler topologies, including the processes $e^+e^- \to K^+K^-$, where a resonance with a mass of $(2239.2 \pm 7.1 \pm 11.3)$ MeV/c^2 and a width of $(139.8 \pm 12.3 \pm 20.6)$ MeV is seen [33]; $e^+e^- \to \phi K^+K^-$ [34], where a sharp enhancement is observed in the Born cross section lineshape at a center-of-mass (c.m.) energy of $\sqrt{s} = 2.2324$ GeV; $e^+e^- \to \phi\eta'$ [35], where a resonance with a mass of $(2177.5 \pm 5.1 \pm 18.6)$ MeV/c^2 and a width of $(149.0 \pm 15.6 \pm 8.9)$ MeV is seen; $e^+e^- \to \omega\eta$ [38], a resonance with a mass of $(2179 \pm 21 \pm 3)$ MeV/c^2 and a width of $(89 \pm 28 \pm 5)$ MeV is observed with a significance of 6.1σ; $e^+e^- \to \phi\eta$ [36], a resonant structure is observed with parameters determined to be M = $(2163.5 \pm 6.2 \pm 3.0)$ MeV/c^2 and $\Gamma = (31.1^{+21.1}_{-11.6} \pm 1.1)$ MeV; and $e^+e^- \to K^0_S K^0_L$ [37], a resonant structure around 2.2 GeV is observed, with a mass and width of $2273.7 \pm 5.7 \pm 19.3$ MeV/c^2 and $86 \pm 44 \pm 51$ MeV respectively. The Breit-Wigner parameters of $\phi(2170)$ are not consistent between the different studies, especially concerning the width.

In addition, a resonance-like structure called X(2400) might exist around 2.4 GeV in the $\phi\pi^+\pi^-$ cross section line-shape. The X(2400) was first studied by the Belle [4] experiment. Later, Shen and Yuan [39] performed a fit to the X(2400) structure using the combined data of the Belle and BABAR experiments. The mass and the width are determined to be (2436 ± 26) MeV/c^2 and (121 ± 35) MeV, respectively. However, its statistical significance is less than 3σ. An interpretation is proposed for X(2400) as a partner state of the $\phi(2170)$ resonance [40]. Therefore, a precise measurement of $e^+e^- \to \phi\pi^+\pi^-$ is desirable to establish the mass and width of the $\phi(2170)$ resonance and to search for the possible structure near 2.4 GeV.

In this paper, we report the measurement of Born cross

sections for the process $e^+e^- \to \phi\pi^+\pi^-$ at 22 c.m. energies between 2.0000 and 3.0800 GeV.

II. DETECTOR AND DATA SAMPLES

The BESIII detector [41] records symmetric e^+e^- collisions provided by the BEPCII storage ring [42], which operates with a peak luminosity of 1×10^{33} cm^{-2}s^{-1} in the c.m. energy range between 2.0000 and 4.9000 GeV. BESIII has collected large data samples in this energy region [43]. The cylindrical core of the BESIII detector covers 93% of the full solid angle and consists of a helium-based multilayer drift chamber (MDC), a plastic scintillator time-of-flight system (TOF), and a CsI(Tl) electromagnetic calorimeter (EMC), which are all enclosed in a superconducting solenoidal magnet providing a 1.0 T magnetic field. The solenoid is supported by an octagonal flux-return yoke with resistive plate counter muon identification modules interleaved with steel. The charged-particle momentum resolution at 1 GeV/c is 0.5%, and the dE/dx resolution is 6% for electrons from Bhabha scattering. The EMC measures photon energies with a resolution of 2.5% (5%) at 1 GeV in the barrel (end-cap) region. The time resolution in the TOF barrel region is 68 ps, while that in the end-cap region is 110 ps. The end-cap TOF system was upgraded in 2015 using multi-gap resistive plate chamber technology, providing a time resolution of 60 ps [44].

Simulated Monte Carlo (MC) samples of signal and background processes are produced to optimize the event selection criteria, determine the detection efficiency and estimate the background contamination. The response of the detector is reproduced using a GEANT4-based [46] MC simulation software package, which includes the geometric and material description of the BESIII detector, the detector response and digitization models.

Background samples of QED processes are produced with the BABAYAGA [47] generator and inclusive hadronic processes are generated with the LUARLW [48] generator. Signal MC samples of the process $e^+e^- \to \phi\pi^+\pi^-$ with one million events are generated according to the result of a Partial Wave Analysis (PWA) at each energy point (detailed in Sec. V). The signal MC samples are used to determine the reconstruction efficiency, and the correction factors for ISR and vacuum polarization (VP).

III. EVENT SELECTION AND BACKGROUND ANALYSIS

Signal events of the $e^+e^- \to \phi\pi^+\pi^-$ process are reconstructed via the $\phi \to K^+K^-$ decay. Charged track candidates are reconstructed from hits in the MDC and need to satisfy $|\cos\theta| < 0.93$, where θ is the polar angle with respect to the symmetry axis of the MDC. The closest approach to the interaction point is required to be less than 10 cm along the symmetry axis and less than 1 cm in the perpendicular plane. Combined TOF and dE/dx information is used to perform the particle identification (PID), obtaining probabilities for the π, K and p hypotheses. The particle type with the largest probability is assigned to each track. Since the tracking efficiency decreases sharply in the low momentum region below 0.5 GeV/c, and most kaon candidates are expected to have a low momentum, one kaon is allowed to be missing in this study to increase the selection efficiency. A candidate event is, therefore, expected to have two pions and at least one kaon reconstructed.

A vertex fit to the $\pi^+\pi^-K^\pm$ combination is then applied and required to have converged for an event to be kept for further analysis. For events with four charged tracks, both $\pi^+\pi^-K^+$ and $\pi^+\pi^-K^-$ combinations are tested. Under the hypothesis that one kaon is missing, a one-constraint (1C) kinematic fit is performed to the combinations that are kept after the vertex fit. For each event, the $\pi^+\pi^-K^\pm$ combination with the smallest χ^2 of the 1C kinematic fit ($\chi^2_{\rm 1C}(\pi^+\pi^-KK_{miss})$) is retained. Finally, events with $\chi^2_{\rm 1C} \geq 10$ are rejected. After applying the selection criteria, we use the momenta of the particles obtained from the kinematic fit in the further analysis.

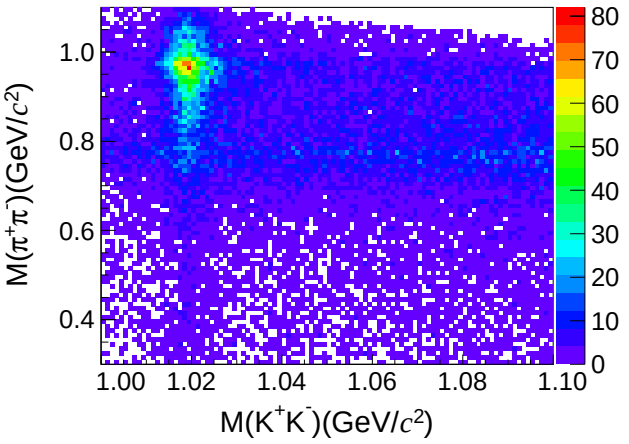

FIG. 1: Distribution of $M_{\pi^+\pi^-}$ versus $M_{K^+K^-}$ for the data at $\sqrt{s} = 2.1250$ GeV.

Events passing the selection criteria described above are shown in Fig. 1 for the data at $\sqrt{s} = 2.1250$ GeV. The invariant mass of the K^+K^- pairs shows a clear signal band around the ϕ mass. The enhancement around 0.98 GeV/c^2 in the $\pi^+\pi^-$ invariant mass indicates a correlation between $f_0(980)$ and ϕ production due to the process $e^+e^- \to \phi f_0(980)$.

The distribution of the K^+K^- invariant mass is shown in Fig. 2. The range of $|M_{K^+K^-} - m_\phi| < 0.01$ GeV/c^2 is regarded as the signal region in the following study, where $m_\phi = 1019.461$ MeV/c^2 is the world average ϕ

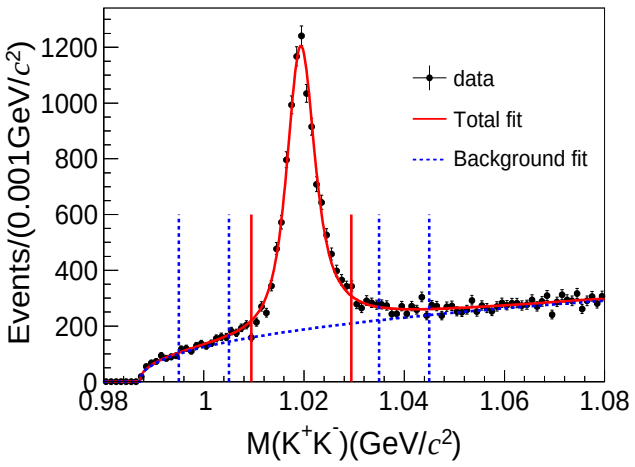

FIG. 2: Fit to the $M_{K^+K^-}$ distribution for the data at $\sqrt{s} = 2.1250$ GeV: the signal is described by a P-wave Breit-Wigner (BW) function convolved with a Gaussian function, and the background is described by a reversed ARGUS function. The range between the two red vertical solid lines is regarded as signal region, and the ranges between the two blue vertical dashed lines on each side of the signal peak are regarded as the sideband regions.

mass from the PDG [1]. The sideband regions, defined as [0.995,1.005] and [1.035,1.045] GeV/c^2, are used to study non-ϕ background contributions.

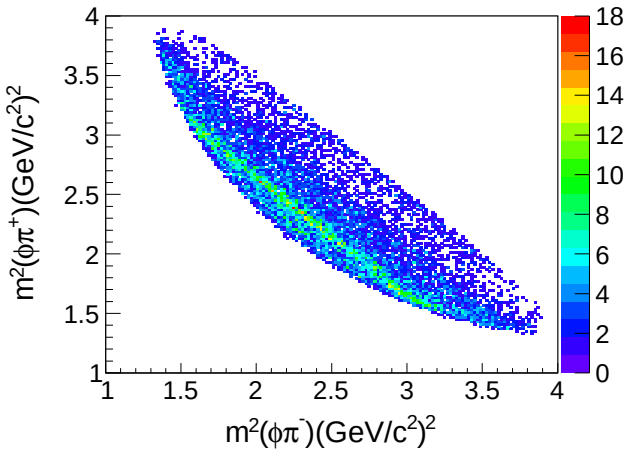

FIG. 3: Dalitz plot of $M_{\phi\pi^+}$ versus $M_{\phi\pi^-}$ for the data at $\sqrt{s} = 2.1250$ GeV.

An accumulation of events exists around the mass of the ρ meson in Fig 1, which can also clearly be seen in the Dalitz plot in Fig. 3. This indicates a non-negligible background contribution from the $e^+e^- \to \rho K^+K^-$ process. In addition, the enhancement due to the $f_0(980)$ can also clearly be seen in the Dalitz plot. Based on a study of the ϕ sideband and an analysis of the inclusive MC sample, the $e^+e^- \to K^*(892)K^\pm\pi^\pm$ process is found to be the dominant background source. Peaking background in the ϕ signal region is negligible.

IV. SIGNAL YIELDS

The $e^+e^- \to \phi\pi^+\pi^-$ signal yields are obtained from unbinned maximum likelihood fits to the K^+K^- invariant mass in the region $[2 \cdot m_{K^\pm}, 1.08]$ GeV/c^2. In the fit, the ϕ peak is modeled as a P-wave BW function convolved with a Gaussian function to account for a difference in detector resolution and an offset in calibration between data and the MC simulation [34]. The P-wave BW function is defined in the form

$$f(m) = |A(m)|^2 \cdot p^{2l+1}, \tag{1}$$

$$A(m) = \frac{1}{m^2 - m_\phi^2 + im\Gamma(m)} \frac{B(p)}{B(p')}, \tag{2}$$

$$\Gamma(m) = \left(\frac{p}{p'}\right)^{2l+1} \left(\frac{m_\phi}{m}\right) \Gamma_\phi \left[\frac{B(p)}{B(p')}\right], \tag{3}$$

$$B(p) = \frac{1}{\sqrt{1 + (Rp)^2}}, \tag{4}$$

where p is the momentum of the kaon in the rest frame of the K^+K^- system, p' is the momentum of the kaon at the ϕ peak mass, and Γ_ϕ is the width of the ϕ resonance [1]. The angular momentum (l) is equal to one, $B(p)$ is the Blatt-Weisskopf form factor, and $R = 3$ GeV^{-1} is the radius of the centrifugal barrier [49].

Since no peaking background is expected in the signal area, the background is parameterized with a reversed ARGUS function [50]. The parameters of the Gaussian function and the reversed ARGUS function are determined in a fit to the data. The fit result for the c.m. energy $\sqrt{s} = 2.1250$ GeV is shown in Fig. 2. We obtain a similar fit quality for all c.m. energies.

V. CROSS-SECTION CALCULATION

The Born cross section is calculated by:

$$\sigma^B = \frac{N^{obs}}{\mathcal{L} \cdot (1 + \delta^\gamma) \cdot 1/|1 - \Pi|^2 \cdot \epsilon \cdot \mathcal{B}}, \tag{5}$$

where N^{obs} is the signal yield; $\mathcal{L}$ is the integrated luminosity; $(1+\delta^{\gamma})$ is the initial-state radiation (ISR) correction factor and $1/|1-\Pi|^2$ is the vacuum-polarization factor; ϵ is the detection efficiency; and $\mathcal{B}$ is the branching fraction of the decay $\phi \to K^+K^-$, $\mathcal{B}(\phi \to K^+K^-) = (49.2 \pm 0.5)\%$ [1].

In the following, we will refer to the combination of the ISR and VP correction factors as the radiative-correction factor. It is obtained in CONEXC [51] by parameterizing the ISR production of a final state X using

$$\sigma_{e^+e^-\to\gamma_{\rm ISR}X(s)} = \int d\sqrt{s'}\frac{2\sqrt{s'}}{s}W(s,x)\frac{\sigma_B(s')}{[1-\Pi(s')]^2}, \quad (6)$$

where $\sqrt{s'}$ is the effective c.m. energy of the final state with $s' = s(1-x)$ and x is the effective fraction of the beam energy carried by photons emitted from the initial state ($x = 2E_\gamma/\sqrt{s}$); and $W(s,x)$ is the probability density function for radiating an ISR photon with $E_\gamma = x\sqrt{s}/2$. The VP effect including the contributions from leptons and quarks, is described by $\Pi(s')$. Here $\sigma_B(s')$ is the input Born cross section. The radiative correction factor is obtained through $(1+\delta) = \sigma_{e^+e^-\to\gamma X}(s)/\sigma_B(s)$.

To adequately describe the data in our MC simulation, the PWA MC sample is generated at each energy point. For a few low-statistic points, the PWA parameters obtained at the most adjacent high-statistic energies are applied. The quasi-two-body decay amplitudes in the sequential decays are constructed using covariant tensor amplitudes [52]. The $e^+e^- \to \phi\pi^+\pi^-$ process is found to be well described by four subprocesses: $e^+e^- \to \phi f_0(980)$, $\phi\sigma$, $\phi f_0(1370)$ and $\phi f_2(1270)$. The intermediate states are parametrized with relativistic BW functions, except for the σ and $f_0(980)$, which are described with using the model described in [54] and by a Flatté formula [53], respectively. The resonance parameters of the $f_0(980)$ and the wide resonance σ in the fit are fixed to those in Ref. [53] and Refs. [53, 54], respectively, and those of other intermediate states are fixed to the PDG values. The relative magnitudes and phases of the individual intermediate processes are determined by performing an unbinned maximum likelihood fit using MINUIT [55]. To describe the background below the ϕ peak, sideband events are added to the likelihood with negative weights.

The signal MC simulation based on the PWA results has reasonable agreement with the experimental data at all the c.m. energies. The comparison of the MC simulation and experimental data for the $M(\pi^+\pi^-)$ distribution at $\sqrt{s} = 2.1250$ GeV is shown in Fig. 4.

The efficiency ϵ and the correction factor $(1+\delta^{\gamma})$ depend on the input cross section line-shape and need to be determined using an iterative procedure. The BABAR result [5] is used as the initial input cross section and

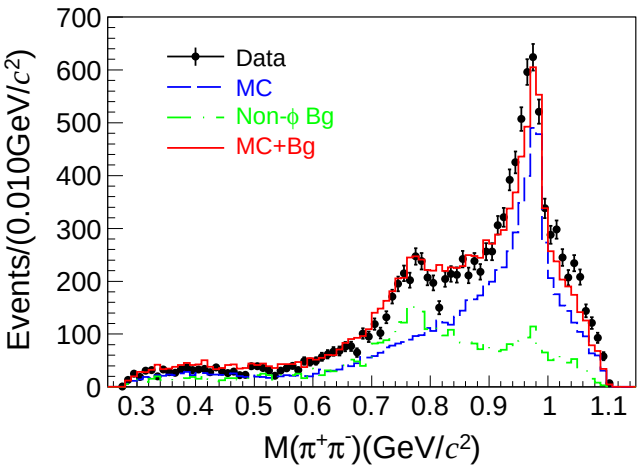

FIG. 4: Invariant mass distribution of the $\pi^+\pi^-$ candidates for the data at $\sqrt{s} = 2.1250$ GeV. The black dots with uncertainties are experimental data, the blue dashed line is the signal MC distribution following the PWA solution, the green dash-dotted line is the non-ϕ background estimated from the ϕ sideband region and the red solid line is the sum of the former two distributions.

the updated Born cross section is obtained through the resulting MC simulation. We repeat this procedure, using the newly determined Born cross sections as the new input, until the measured Born cross section converges.

The Born cross section for $e^+e^- \to \phi\,\pi^+\pi^-$ at each energy point is listed in Table I and shown in Fig. 5.

VI. SYSTEMATIC UNCERTAINTY

Systematic uncertainties in the cross section measurement come from the luminosity measurement, tracking efficiency, PID efficiency, kinematic fit, signal and background shape, fitting range, radiative correction, MC sample size and the branching fraction of the decay $\phi \to K^+K^-$.

1. The integrated luminosity is measured using large angle Bhabha events, with an uncertainty of 1.0% [45].

2. The tracking efficiency uncertainty is estimated to be 1.0% for each track [34]. Thus, 3.0% is taken as the systematic uncertainty for the two pion and one kaon tracks.

3. The PID efficiency uncertainty is estimated to be 1.0% per $\pi^{\pm}$ and 1.0% per $K^{\pm}$ [34]. So 3.0% is taken as the systematic uncertainty on the PID efficiency.

TABLE I: Cross sections of the process $e^+e^- \to \phi\pi^+\pi^-$ at different c.m. energies. N^{obs} is the yield of signal events, $\sqrt{s}$ is the c.m. energy, $\mathcal{L}$ the integrated luminosity, $1+\delta^\gamma$ the initial radiative correction factor, $1/[1-\Pi]^2$ the vacuum polarization factor, ϵ the detection efficiency and σ^B the Born cross section. The first uncertainties are statistical and the second systematic.

$\sqrt{s}$ (GeV)	$\mathcal{L}$ (pb^{-1})	N^{obs}	$(1+\delta^\gamma)$	$1/\|1-\Pi\|^2$	ϵ	σ^B(pb)
2.0000	10.1	577.0 ± 46.8	0.979	1.037	0.3358	341.2 ± 27.7 ± 24.4
2.0500	3.34	191.5 ± 24.6	0.962	1.038	0.3767	312.9 ± 40.2 ± 20.5
2.1000	12.2	1100.7 ± 51.1	0.949	1.039	0.3976	464.4 ± 21.6 ± 24.3
2.1250	108.	9372.1 ± 144.1	0.950	1.039	0.4166	431.1 ± 6.6 ± 23.3
2.1500	2.84	220.0 ± 20.0	0.964	1.040	0.3736	423.5 ± 38.5 ± 31.7
2.1750	10.6	760.8 ± 39.1	1.005	1.040	0.3742	379.3 ± 19.5 ± 24.4
2.2000	13.7	706.1 ± 38.3	1.077	1.040	0.3655	254.8 ± 13.8 ± 18.9
2.2324	11.9	435.2 ± 29.5	1.189	1.041	0.3344	176.6 ± 12.0 ± 14.6
2.3094	21.1	587.3 ± 37.7	1.187	1.041	0.3602	130.8 ± 8.4 ± 6.5
2.3864	22.5	697.3 ± 37.0	1.128	1.041	0.3890	138.8 ± 7.4 ± 8.4
2.3960	66.9	1977.7 ± 65.5	1.128	1.041	0.3910	132.0 ± 4.4 ± 7.6
2.5000	1.10	18.7 ± 5.2	1.212	1.040	0.3777	74.2 ± 20.6 ± 5.0
2.6444	33.7	501.0 ± 33.2	1.311	1.039	0.3376	66.6 ± 4.4 ± 4.6
2.6464	34.0	423.4 ± 29.8	1.312	1.039	0.3360	56.6 ± 4.0 ± 3.9
2.7000	1.03	22.0 ± 6.1	1.636	1.039	0.3292	83.3 ± 23.1 ± 5.9
2.8000	1.01	11.6 ± 4.1	1.446	1.037	0.3141	48.8 ± 17.2 ± 7.8
2.9000	105.	687.0 ± 37.7	1.452	1.033	0.3014	30.1 ± 1.6 ± 1.8
2.9500	15.9	114.4 ± 14.5	1.468	1.029	0.2958	33.9 ± 4.3 ± 2.3
2.9810	16.1	72.4 ± 15.2	1.478	1.025	0.2972	21.1 ± 4.4 ± 1.4
3.0000	15.9	74.6 ± 13.4	1.485	1.021	0.2899	22.4 ± 4.0 ± 1.8
3.0200	17.3	78.2 ± 12.2	1.494	1.014	0.2877	21.8 ± 3.4 ± 1.6
3.0800	126.	576.9 ± 34.8	1.586	0.915	0.2732	24.7 ± 1.5 ± 1.4

4. The uncertainty from the kinematic fit comes from the inconsistency between the data and MC simulation of the helix parameters. Following the procedure described in Ref. [57], the helix parameters for the charged tracks of MC samples are corrected to eliminate the inconsistency during uncertainty study. The agreement of χ^2 distributions between data and the MC simulation is significantly improved. Half of the difference between the selection efficiencies with and without the helix parameter correction is taken as the systematic uncertainty.

5. Uncertainties due to the choice of signal shape, background shape and fitting range are estimated by introducing the changes below. The ϕ signal is described by a P-wave BW function convolved with a Gaussian function. To estimate the signal shape uncertainty, the signal shape is changed to the shape from the signal MC simulation convolved with a Gaussian function and the resulting difference is taken as the uncertainty from the signal model. To estimate the background model uncertainty the background function is modified from a reversed ARGUS function to the function of $f(M) = (M - M_a)^c(M_b - M)^d$, where M_a and M_a are the lower and upper edges of the mass distribution while c and d are the parameters which were determined in the fit. The fit range is extended from [0.98, 1.08] GeV/c^2 to [0.98, 1.10] GeV/c^2 to estimate the fit-range uncertainty. The differences between the number of signal events before and after the changes are taken as the systematic uncertainties.

6. Uncertainties in the possible distortions of the cross section line-shape introduce systematic uncertainties in the radiative correction factor and the efficiency. These are estimated by using the cross section line-shape function $\sigma = \sigma(\sqrt{s}; p_1, p_2, ...)$ obtained from the iteration described in Sec. V, where $p_i (i = 1, 2, ...)$ are the parameters which are determined in the fit. All parameters are randomly varied within their uncertainties and the resulting parametrization of the line-shape is used to recalculate $(1 + \delta)$, ϵ and the corresponding cross sections. This procedure is repeated 1000 times and the standard deviation of the resulting cross sections is taken as a systematic uncertainty.

7. The uncertainty from the MC sample size is estimated by the number of generated events.

8. The uncertainty in $\mathcal{B}(\phi \to K^+K^-)$ is taken from the PDG [1].

We list the systematic uncertainty sources and their contributions for all c.m. energies in Table II. All systematic uncertainty sources are assumed independent and summed in quadrature.

TABLE II: Relative systematic uncertainties (in %) associated with the integrated luminosity ($\mathcal{L}$), the tracking efficiency (ϵ_{tr}), the PID efficiency (PID), the kinematic fit (KF), ϕ signal shape (Sig), background shape (Bkg), fit range (FR), the initial state radiation and the vacuum polarization correction factor (1+δ), the MC statistics (Δ_{MC}) and the branching fraction ($\mathcal{B}$). The total uncertainty is obtained by summing the individual contributions in quadrature.

$\sqrt{s}$(GeV)	$\mathcal{L}$	ϵ_{tr}	PID	KF	Sig	Bkg	FR	(1+δ)	Δ_{MC}	$\mathcal{B}$	Total
2.0000	1.0	3.0	3.0	2.1	5.0	0.4	1.5	0.1	0.4	1.0	7.2
2.0500	1.0	3.0	3.0	2.2	3.7	0.8	1.6	1.2	0.4	1.0	6.6
2.1000	1.0	3.0	3.0	2.2	1.0	0.1	0.1	0.5	0.4	1.0	5.2
2.1250	1.0	3.0	3.0	1.9	2.1	0.8	0.3	0.2	0.1	1.0	5.4
2.1500	1.0	3.0	3.0	2.0	4.9	0.7	2.9	0.0	0.4	1.0	7.6
2.1750	1.0	3.0	3.0	2.1	3.5	0.7	2.0	0.2	0.4	1.0	6.4
2.2000	1.0	3.0	3.0	2.1	5.8	0.0	0.2	0.1	0.4	1.0	7.7
2.2324	1.0	3.0	3.0	2.3	6.1	0.3	2.1	0.4	0.5	1.0	8.2
2.3094	1.0	3.0	3.0	1.8	1.6	0.6	0.5	0.2	0.4	1.0	5.2
2.3864	1.0	3.0	3.0	1.9	0.1	0.5	3.4	0.1	0.4	1.0	6.0
2.3960	1.0	3.0	3.0	1.8	3.2	0.7	0.8	0.4	0.4	1.0	5.9
2.5000	1.0	3.0	3.0	1.8	4.4	0.5	0.6	0.0	0.4	1.0	6.6
2.6444	1.0	3.0	3.0	1.8	5.4	0.4	0.5	0.0	0.4	1.0	7.3
2.6464	1.0	3.0	3.0	1.8	5.3	0.0	0.5	0.6	0.4	1.0	7.3
2.7000	1.0	3.0	3.0	1.9	5.0	0.5	0.5	0.6	0.4	1.0	7.1
2.8000	1.0	3.0	3.0	1.8	3.3	0.7	0.7	0.2	0.5	1.0	6.0
2.9000	1.0	3.0	3.0	1.7	3.7	0.3	0.3	0.4	0.4	1.0	6.1
2.9500	1.0	3.0	3.0	1.6	5.8	0.3	0.8	0.4	0.4	1.0	7.6
2.9810	1.0	3.0	3.0	1.8	4.0	0.7	3.7	0.6	0.5	1.0	7.4
3.0000	1.0	3.0	3.0	1.5	6.9	0.4	2.1	0.2	0.5	1.0	8.7
3.0200	1.0	3.0	3.0	1.6	5.6	1.2	1.1	0.2	0.5	1.0	7.6
3.0800	1.0	3.0	3.0	1.7	3.7	0.9	0.3	0.6	0.6	1.0	6.2

VII. LINE-SHAPE FITTING OF $e^+e^- \to \phi\pi^+\pi^-$

The measured Born cross sections are shown in Fig. 5 together with results from the BABAR and Belle experiments. A clear structure and an enhancement can be seen at around 2.1 and 2.4 GeV, respectively, where the first is identified as the $\phi(2170)$ resonance and the second is denoted as X(2400).

A least χ^2 fit, incorporating the correlated and uncorrelated uncertainties, is performed on the cross sections measured in this work to determine the parameters of these resonances. The fit function used here is

$$\sigma^B = |BW_1 + BW_2 \cdot e^{i\cdot\theta_2} + BW_3 \cdot e^{i\cdot\theta_3}|^2, \qquad (7)$$

where BW_i takes the form [39]

$$BW(\sqrt{s}) = \sqrt{\frac{M^2}{s}}\frac{\sqrt{12\pi\Gamma_{e^+e^-}\mathcal{B}(R\to f)\Gamma_{tot}}}{s - M^2 + iM\Gamma_{tot}} \cdot ps, \qquad (8)$$

as the BW function for the resonances $\phi(1680)$, $\phi(2170)$ and X(2400). Here $\phi(1680)$ denotes a resonance observed by BABAR and Belle around 1.7 GeV, which is clearly visible in Fig. 5; $\phi(2170)$ and X(2400) denote structures around 2.1 GeV and 2.4 GeV, respectively; and θ_i in Eq.(7) is the phase between the $\phi(1680)$ and the other two resonances. In Eq.(8), M is the mass of the resonance, Γ_{tot} and $\Gamma_{e^+e^-}$ are the total width and electronic width, respectively, $\mathcal{B}(R \to f)$ is the branching fraction of R decays into final state f, and $ps = \sqrt{PS(\sqrt{s})/PS(M)}$, where $PS(\sqrt{s})$ is the three-body decay phase space factor of $R \to \phi\pi^+\pi^-$. Here, the total width is a constant.

In the fit to the cross section line-shape, both statistical and systematic uncertainties are taken into account. Uncertainties from the luminosity, the tracking and PID efficiency, the kinematic fit, the radiative correction factor, the MC simulation sample size and the branching fraction are assumed to be fully correlated across the whole range in $\sqrt{s}$, and the remaining uncertainties are treated as uncorrelated. In this fit, the parameters of $\phi(1680)$ are fixed to be M($\phi(1680)$) = 1681 MeV/c^2 and $\Gamma(\phi(1680))$ = 221 MeV, which are obtained by a fit on combined $e^+e^- \to \phi\pi^+\pi^-$ cross section data of Belle and BABAR [39].

The resulting fit curve is shown in Fig. 5. It has a goodness-of-fit of χ^2/ndf = 19/(22-9), where ndf is the number of degrees of freedom. The statistical significance of the third Breit-Wigner used to describe the structure at 2.4 GeV is estimated to be 8.5σ from the change in

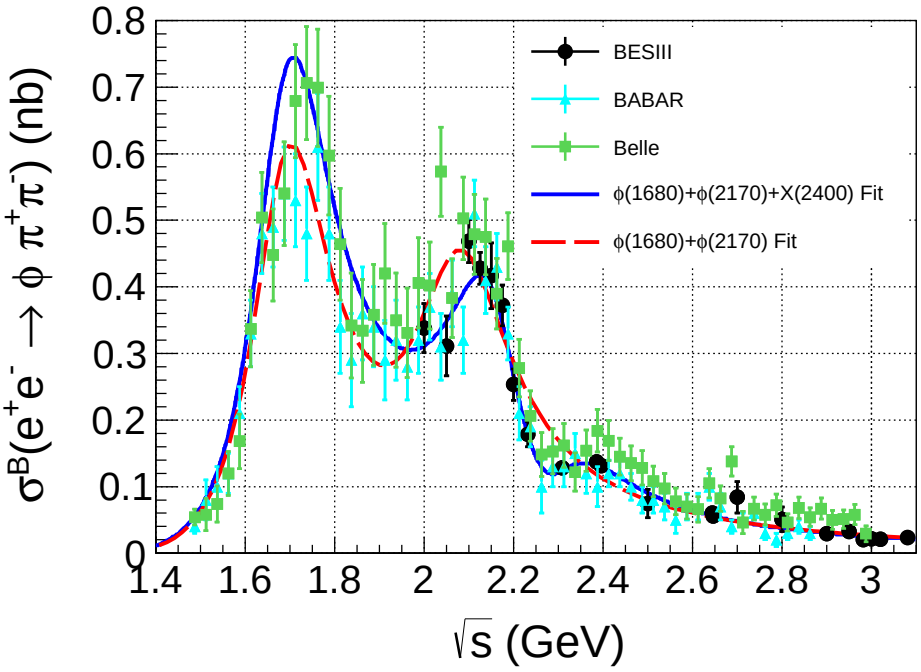

FIG. 5: Born cross section of the $e^+e^- \to \phi\pi^+\pi^-$ process as a function of the c.m. energy. The light blue triangles and green squares with uncertainties show the results from BABAR and Belle respectively. The black dots with error bars are results from this work. The dark blue curve shows the result of the fit to the black data points using Eq.(7). Comparing with the red dashed line, which comes from a fit excluding the X(2400) contribution, the result with three resonances describes the cross section line-shape much better.

the χ^2 values when this contribution is removed. We obtain four ambiguous solutions with equal fit quality. The parameters of all four are shown in Table III.

The systematic uncertainties of the resonance parameters mainly come from the cross section fitting. The uncertainties associated with the fit procedure include effects from the choice of $\phi(1680)$ model. To estimate the uncertainty from the choice of $\phi(1680)$ model, the mass and width of $\phi(1680)$ are fixed to the PDG average parameters [1]. The difference of the fit result is considered as the systematic uncertainty. The systematic uncertainties of the $\phi(2170)$ resonance mass and width are obtained to be 4 MeV/c^2 and 5 MeV, while for X(2400) mass and width we find 6 MeV/c^2 and 6 MeV, respectively.

VIII. CONCLUSION

In summary, we have measured the Born cross section of the $e^+e^- \to \phi\pi^+\pi^-$ process using data samples collected with the BESIII detector at 22 c.m. energies from 2.0000 GeV to 3.0800 GeV. The measured cross section is consistent with previous results from the BABAR [5], Belle [4] and BESIII [56] experiments, but with improved precision.

For the cross section line-shape, a least χ^2 fit is performed to study possible resonant contributions. The $\phi(2170)$ resonance is observed, with a mass of $(2158^{+30}_{-33} \pm 4)$ MeV/c^2 and a width of $(218^{+81}_{-64} \pm 5)$ MeV, where the first uncertainties are statistical and the second systematic. The central value of the $\phi(2170)$ width obtained in this work is the largest among all existing results [3–7]. Our result is close to that found in Ref. [39], but as we fix the $\phi(1680)$ mass and width to the fit result of that study, the obtained parameters are correlated. An independent data sample in the $\phi(1680)$ mass region is necessary to further elucidate this question.

In addition, another structure X(2400) is observed at around 2.4 GeV. Comparing our fit with and without a Breit-Wigner to account for the X(2400), we find a statistical significance of 8.5σ in favor of including the third Breit-Wigner resonance. We obtained a mass of $(2298^{+60}_{-44} \pm 6)$ MeV/c^2 and a width of $(219^{+117}_{-112} \pm 6)$ MeV for the X(2400) structure, where the first uncertainties are statistical and the second systematic. The uncertainties of the X(2400) parameters are large in this work. This is a result of the lack of energy points in the 2.4 GeV region. Collecting additional data samples in this region will help to reduce these uncertainties. Moreover, since the structure at 2.4 GeV has also been seen in the $K^+K^-f_0(980)$ mode with $f_0(980) \to \pi^+\pi^-$ and $\pi^0\pi^0$ [2], a future study of this channel with a more robust amplitude analysis will

TABLE III: Results of fit to the $e^+e^- \to \phi\pi^+\pi^-$ cross section measured in this work. The uncertainties are statistical only. M, Γ_{tot}, and $\mathcal{B}\cdot\Gamma_{e^+e^-}$ are the mass (in MeV/c^2), total width (in MeV) and the product of the branching fraction to $\phi\pi^+\pi^-$ and the e^+e^- partial width (in eV), respectively. ϕ is the relative phase (in radians).

Parameters	Solution I	Solution II	Solution III	Solution IV
$\mathcal{B}\cdot\Gamma_{e^+e^-}(\phi(1680))$	$25.4\ ^{+31.6}_{-13.6}$	$44.3\ ^{+14.1}_{-31.1}$	$29.0\ ^{+29.4}_{-15.8}$	$48.1\ ^{+10.3}_{-34.9}$
$M(\phi(2170))$		$2158\ ^{+30}_{-33}$		
$\Gamma_{tot}(\phi(2170))$		$218\ ^{+81}_{-64}$		
$\mathcal{B}\cdot\Gamma_{e^+e^-}(\phi(2170))$	$15.4\ ^{+1116.0}_{-11.3}$	$77.4\ ^{+1056.4}_{-70.9}$	$56.5\ ^{+1077.3}_{-50.0}$	$244.2\ ^{+889.6}_{-237.7}$
ϕ_1	$1.87\ ^{+1.34}_{-0.57}$	$-1.88\ ^{+0.92}_{-0.50}$	$2.32\ ^{+0.93}_{-0.98}$	$-1.47\ ^{+0.51}_{-0.91}$
$M(X(2400))$		$2298\ ^{+60}_{-44}$		
$\Gamma_{tot}(X(2400))$		$219\ ^{+117}_{-112}$		
$\mathcal{B}\cdot\Gamma_{e^+e^-}(X(2400))$	$4.2\ ^{+983.4}_{-3.5}$	$13.0\ ^{+976.9}_{-11.5}$	$64.2\ ^{+924.2}_{-62.7}$	$167.6\ ^{+820.8}_{-166.1}$
ϕ_2	$0.07\ ^{+1.02}_{-1.18}$	$-3.03\ ^{+1.34}_{-1.40}$	$-0.59\ ^{+0.45}_{-0.57}$	$2.61\ ^{+1.98}_{-0.76}$

be helpful to improve knowledge of the X(2400) state.

Acknowledgments

The BESIII collaboration thanks the staff of BEPCII, the IHEP computing center and the super computing center of USTC for their strong support. This work is supported in part by National Key Basic Research Program of China under Contracts Nos. 2020YFA0406400, 2020YFA0406300; National Natural Science Foundation of China (NSFC) under Contracts Nos. 11625523, 11635010, 11735014, 11822506, 11835012, 11935015, 11935016, 11935018, 11961141012, 12022510, 12025502, 12035009, 12035013, 12061131003, 11705192, 11950410506, 12061131003; the Chinese Academy of Sciences (CAS) Large-Scale Scientific Facility Program; Joint Large-Scale Scientific Facility Funds of the NSFC and CAS under Contracts Nos. U1732263, U1832207, U1832103, U2032111; CAS Key Research Program of Frontier Sciences under Contract No. QYZDJ-SSW-SLH040; 100 Talents Program of CAS; INPAC and Shanghai Key Laboratory for Particle Physics and Cosmology; ERC under Contract No. 758462; European Union Horizon 2020 research and innovation programme under Contract No. Marie Sklodowska-Curie grant agreement No 894790; German Research Foundation DFG under Contracts Nos. 443159800, Collaborative Research Center CRC 1044, FOR 2359, FOR 2359, GRK 214; Istituto Nazionale di Fisica Nucleare, Italy; Ministry of Development of Turkey under Contract No. DPT2006K-120470; National Science and Technology fund; Olle Engkvist Foundation under Contract No. 200-0605; STFC (United Kingdom); The Knut and Alice Wallenberg Foundation (Sweden) under Contract No. 2016.0157; The Royal Society, UK under Contracts Nos. DH140054, DH160214; The Swedish Research Council; U. S. Department of Energy under Contracts Nos. DE-FG02-05ER41374, DE-SC-0012069

[1] P.A. Zyla *et al.* (Particle Data Group), Prog. Theor. Exp. Phys. **2020**, 083C01 (2020).
[2] B. Aubert *et al.* (BABAR Collaboration), Phys. Rev. D **74**, 091103(R) (2006); **76**, 012008 (2007).
[3] M. Ablikim *et al.* (BES Collaboration), Phys. Rev. Lett. **100**, 102003 (2008).
[4] C. P. Shen *et al.* (Belle Collaboration), Phys. Rev. D **80**, 031101(R) (2009).
[5] J. P. Lees *et al.* (BABAR Collaboration), Phys. Rev. D **86**, 012008 (2012).
[6] M. Ablikim *et al.* (BESIII Collaboration), Phys. Rev. D **91**, 052017 (2015).
[7] M. Ablikim *et al.* (BESIII Collaboration), Phys. Rev. D **99**, 012014 (2019).

[8] G. J. Ding and M. L. Yan, Phys. Lett. B **650**, 390 (2007).
[9] G. J. Ding and M. L. Yan, Phys. Lett. B **657**, 49 (2007).
[10] X. Wang *et al.*, Phys. Rev. D **85**, 074024 (2012).
[11] S. S. Afonin and I. V. Pusenkov, Phys. Rev. D **90**, 094020 (2014).
[12] C. Q. Pang, Phys. Rev. D **99**, 074015 (2019).
[13] C. G. Zhao *et al.*, Phys. Rev. D **99**, 114014 (2019).
[14] Q. Li *et al.*, arXiv:2004.05786.
[15] J. Ho, R. Berg, T.G. Steele, W. Chen, and D. Harnett, Phys. Rev. D **100**, 034012 (2019).
[16] Z. G. Wang, Nucl. Phys. A **791**, 106 (2007).
[17] H. X. Chen *et al.*, Phys. Rev. D **78**, 034012 (2008).
[18] N. V. Drenska, R. Faccini and A. D. Polosa, Phys. Lett. B **669**, 160 (2008).
[19] C. R. Deng, J. L. Ping, and T. Goldman, Phys. Rev. D **82**, 074001 (2010).
[20] H. W. Ke and X. Q. Li, Phys. Rev. D **99**, 036014 (2019).
[21] S. S. Agaev, K. Azizi, and H. Sundu, Phys. Rev. D **101**, 074012 (2020).
[22] R. R. Dong *et al.*, Eur. Phys. J. C **80**, 749 (2020).
[23] F. X. Liu *et al.*, arXiv:2008.01372.
[24] E. Klempt and A. Zaitsev, Phys. Rep. **454**, 1 (2007).
[25] L. Zhao *et al.*, Phys. Rev. D **87**, 054034 (2013).
[26] C. Deng *et al.*, Phys. Rev. D **88**, 074007 (2013).
[27] Y. B. Dong *et al.*, Phys. Rev. D **96**, 074027 (2017).
[28] Y. L. Yang, D. Y. Chen, and Z. Lu, Phys. Rev. D **100**, 073007 (2019).
[29] A. Martinez Torres *et al.*, Phys. Rev. D **78**, 074031 (2008).
[30] S. Gomez-Avila, M. Napsuciale and E.Oset, Phys. Rev. D **79**, 034018 (2009).
[31] B. Aubert *et al.*, Phys. Rev. D **77**, 092002 (2008).
[32] M. Ablikim *et al.* (BESIII Collaboration), Phys. Rev. Lett. **124**, 112001 (2020).
[33] M. Ablikim *et al.* (BESIII Collaboration), Phys. Rev. D **99**, 032001 (2019).
[34] M. Ablikim *et al.* (BESIII Collaboration), Phys. Rev. D **100**, 032009 (2019).
[35] M. Ablikim *et al.* (BESIII Collaboration), Phys. Rev. D **102**, 012008 (2020).
[36] M. Ablikim *et al.* (BESIII Collaboration), Phys. Rev. D **104**, 032007 (2021).
[37] M. Ablikim *et al.* (BESIII Collaboration), Phys. Rev. D **104**, 092014 (2021).
[38] M. Ablikim *et al.* (BESIII Collaboration), arXiv:2009.08099.
[39] C. P. Shen and C. Z. Yuan, Chin. Phys. C **34**, 1045 (2010).
[40] H. X. Chen, C. P. Shen and S. L. Zhu, Phys. Rev. D **98**, 014011 (2018).
[41] M. Ablikim *et al.* (BESIII Collaboration), Nucl. Instrum. Meth. A **614**, 345 (2010).
[42] C. H. Yu *et al.*, Proceedings of IPAC2016, Busan, Korea, 2016, doi:10
[43] M. Ablikim *et al.* (BESIII Collaboration), Chin. Phys. C **44**, 040001 (2020).
[44] X. Li *et al.*, Rad. Det. Tech. Meth. **1**, 13 (2017); Y. X. Guo *et al.*, Radiat. Detect. Technol. Methods **1**, 15 (2017); P. Cao *et al.*, Nucl. Instrum. Meth. A **953**, 163053 (2020).
[45] M. Ablikim *et al.* (BESIII Collaboration), Chin. Phys. C 41, 063001 (2017).
[46] S. Agostinelli *et al.* (GEANT4 Collaboration), Nucl. Instrum. Meth. A **506**, 250 (2003).
[47] G. Balossini, C. M. C. Calame, G. Montagna, O. N. F. Phiccinini, Nucl. Phys. B **758**, 227 (2006).
[48] B. Andersson and H. M. Hu, arXiv:hep-ph/9910285.
[49] F. V. Hippel and C. Quigg, Phys. Rev. D **5**, 624 (1972)
[50] H. Albrecht et al. (ARGUS Collaboration), Phys. Lett. B **340**, 217 (1994).
[51] R. G. Ping *et al.*, Chin. Phys. C **40**, 113002 (2016).
[52] B.S. Zou and D.V. Bugg, Phys. J. A **16**, 537 (2003).
[53] M. Ablikim *et al.* (BES Collaboration), Phys. Lett. B **598**, 149 (2004).
[54] M. Ablikim *et al.* (BES Collaboration), Phys. Lett. B **645**, 19 (2004).
[55] F. James and M. Roos, Comput. Phys. Commun. **10**, 343 (1975).
[56] M. Ablikim *et al.* (BESIII Collaboration), Phys. Rev. D **99**, 011101(R) (2019).
[57] M. Ablikim *et al.* (BESIII Collaboration), Phys. Rev. D **87**, 012002 (2013).